Gradient-extended brittle damage modeling

Thank Thank Nguyen[1][*], Marek Fassin[2], Robert Eggersmann[2], Stefanie Reese[2], and Stephan Wulfinghoff[1]

[1] Kiel University, Institute for Materials Science, Computational Materials Science, Kaiserstr. 2, 24143 Kiel, Germany

[2] RWTH Aachen University, Institute of Applied Mechanics, Mies-van-der-Rohe Str. 1, 52074 Aachen, Germany

Abstract: An elastic-brittle anisotropic model is presented based on the work by Fassin et al. (2019a). After discussing the local model equations and the incorporation of crack-closure, the gradient extension using the micromorphic approach according to Forest (2009) is briefly summarized. In order to run unit cell simulations on the microlevel, relevant material parameters have to be identified. Therefore, the energy dissipation provides a differential equation with a linear and quadratic term for the damage variable. Finally, the isotropic damage model is used to show numerical examples with variation of fracture toughness and volume fraction of pores.

Keywords: anisotropic damage, gradient damage, micromorphic approach

1 Introduction

Due to the renewable energy act proposed by the German government, a significant amount of electric power must be covered by renewable energies. However, a huge amount of the electric power supply will still be provided by fossil power plants. The repeated turn on and off procedures of fossil power plant generators are associated with high demands on the materials' strength in cyclic loading. This can be accounted for by making use of innovative materials which are characterized by improved functional properties and higher performance. In this context, carbon fiber-reinforced (CFR) epoxy resin has widely been used. Before such materials can be applied in the generators, their material behavior and performance must be analyzed. Since the overall mechanical behavior of such heterogeneous media is to a large extent determined by the micro-structure, numerical simulations can be conducted to study the local material behavior and the effective constitutive response. In particular, the initiation and growth of damage at the micro-scale is crucial and needs to be taken care of. Due to the manufacturing processes, micro-cracks and -voids (Fig. 1) are present which grow and coalesce under certain loadings leading to damage processes in the matrix material.

2 Model equation

This section briefly presents the anisotropic gradient-extended damage model, recently published in Fassin et al. (2019a) and its extension to tension compression asymmetry (Fassin et al. (2019b)).

2.1 Local damage model

The free energy density ψ is assumed to consist of three parts

$$\psi = \psi_{\mathrm{e}}(\boldsymbol{\varepsilon}, \boldsymbol{D}) + \underbrace{\psi_{\mathrm{h}}^{\alpha}(\alpha) + \psi_{\mathrm{h}}^{\boldsymbol{D}}(\boldsymbol{D})}_{\psi_{\mathrm{h}}}, \tag{1}$$

representing the elastic, the damage hardening and an additional hardening term with the strain tensor $\boldsymbol{\varepsilon}$, the hardening variable α and the symmetric second order damage tensor $\boldsymbol{D}$. The elastic strain energy for an initially isotropic and material is also split into three parts

$$\psi_{\mathrm{e}}(\boldsymbol{\varepsilon}, \boldsymbol{D}) = \underbrace{\tfrac{1}{2}(1-g)\lambda \mathrm{tr}^2(\boldsymbol{\varepsilon})}_{\lambda\text{-term}} + \underbrace{(1-\vartheta)(1-g)\mu \boldsymbol{I} : \boldsymbol{\varepsilon}^2}_{\mu_{\mathrm{iso}}\text{-term}} + \underbrace{\vartheta\mu(\boldsymbol{I} - \boldsymbol{D}) : \boldsymbol{\varepsilon}^2}_{\mu_{\mathrm{aniso}}\text{-term}} \tag{2}$$

with $g = f(\mathrm{tr}(\boldsymbol{D})) \to$ e.g. $g = \mathrm{tr}(\boldsymbol{D})/3$, μ and λ are the Lamé parameters. The λ-term and μ_{iso}-term are related to isotropic damage since the terms are damaged by the scalar $(1 - g(\boldsymbol{D}))$. The material parameter ϑ controls the degree of damage anisotropy related to both μ-terms: For the choice $\vartheta = 0$, the third term in Eq. (2) vanishes and fully isotropic damage is obtained. In contrast, fully anisotropic damage is achieved for $\vartheta = 1$ and the second term vanishes. Thus, for $\vartheta = 0$ we obtain

doi: 10.24352/UB.OVGU-2020-013

$$\psi_{\mathrm{e}}(\boldsymbol{\varepsilon}, \boldsymbol{D}) = \frac{1}{2}(1-g)\lambda\mathrm{tr}^2(\boldsymbol{\varepsilon}) + \mu(\boldsymbol{I}-\boldsymbol{D}):\boldsymbol{\varepsilon}^2. \tag{3}$$

The quadratic energy with the hardening parameter K_1 is given in Eq. (4). For anisotropic damage the additional hardening represented by Eq. (5) is a convex function of the eigenvalues D_i of the damage tensor with the property $f \to \infty$ for $D_i \to 1$. Eq. (5) ensures that the eigenvalues of the damage tensor do not exceed the value of 1.

$$\psi_{\mathrm{h}}^{\alpha}(\alpha) = \frac{1}{2}K_1\,\alpha^2 \tag{4}$$

$$\psi_{\mathrm{h}}^{\boldsymbol{D}}(\boldsymbol{D}) = \frac{1}{2}K_{\mathrm{h}}^{\boldsymbol{D}}\sum_{i=1}^{3}f(D_i) \tag{5}$$

$$\tag{6}$$

By evaluating the second law of thermodynamics

$$\mathcal{D} = \boldsymbol{\sigma}:\dot{\boldsymbol{\varepsilon}} - \dot{\psi} = (\boldsymbol{\sigma} - \partial_{\boldsymbol{\varepsilon}}\psi_{\mathrm{e}}):\dot{\boldsymbol{\varepsilon}} - \partial_{\boldsymbol{D}}\psi:\dot{\boldsymbol{D}} - \partial_{\alpha}\psi\cdot\dot{\alpha} \geq 0 \tag{7}$$

the thermodynamically conjugate forces like the stress can be derived

$$\boldsymbol{\sigma} = \frac{\partial\psi}{\partial\boldsymbol{\varepsilon}} = \lambda(1-g)\mathrm{tr}\boldsymbol{\varepsilon}\boldsymbol{I} + \mu[(\boldsymbol{I}-\boldsymbol{D})\boldsymbol{\varepsilon} + \boldsymbol{\varepsilon}(\boldsymbol{I}-\boldsymbol{D})] \tag{8}$$

as well as the damage driving force $\boldsymbol{Y}$

$$\boldsymbol{Y} = -\frac{\partial\psi}{\partial\boldsymbol{D}} = -\frac{\partial\psi_{\mathrm{e}}}{\partial\boldsymbol{D}} - \frac{\partial\psi_{\mathrm{h}}}{\partial\boldsymbol{D}} = \boldsymbol{Y}_{\mathrm{e}} - \boldsymbol{Y}_{\mathrm{h}} \tag{9}$$

$$\boldsymbol{Y}_{\mathrm{e}} = -\frac{\partial\psi_{\mathrm{e}}}{\partial\boldsymbol{D}} = \frac{\lambda}{2}\mathrm{tr}\boldsymbol{\varepsilon}\boldsymbol{I} + \mu\boldsymbol{\varepsilon}^2 \tag{10}$$

$$\boldsymbol{Y}_{\mathrm{h}} = \frac{\partial\psi_{\mathrm{h}}}{\partial\boldsymbol{D}} = K_{\mathrm{h}}^{\boldsymbol{D}}\sum_{i=1}^{3}f'(D_i)\,\boldsymbol{n}_i^{D}\otimes\boldsymbol{n}_i^{D} \tag{11}$$

which is split according to the free energy density function into an elastic and hardening part.
Introducing an initial damage threshold Y_0^c and the abbreviation $\beta = \frac{\partial\psi}{\partial\alpha} = \frac{\partial\psi_{\mathrm{h}}}{\partial\alpha} = K_1\,\alpha$ the damage criterion reads:

$$\Phi = \underbrace{\|\boldsymbol{Y}_{\mathrm{e}} - \boldsymbol{Y}_{\mathrm{h}}\|}_{\boldsymbol{Y}} - (Y_0^c + \beta) \leq 0. \tag{12}$$

Then the following associative evolution equations for the internal variables are chosen

$$\dot{\boldsymbol{D}} = \dot{\lambda}\frac{\partial\Phi}{\partial\boldsymbol{Y}} = \dot{\lambda}\frac{\boldsymbol{Y}}{\|\boldsymbol{Y}\|}, \qquad \dot{\alpha} = -\dot{\lambda}\frac{\partial\Phi}{\partial\beta} = \dot{\lambda} \tag{13}$$

with the Kuhn-Tucker conditions

$$\dot{\lambda} \geq 0, \quad \Phi \leq 0, \quad \dot{\lambda}\Phi = 0. \tag{14}$$

2.2 Tension compression asymmetry

Tension compression asymmetry (TCA) is incorporated in this model as follows. The strain $\boldsymbol{\varepsilon}$ is split into a positive and negative part (compare to Ladeveze and Lemaitre (1984))

$$\boldsymbol{\varepsilon} = \boldsymbol{\varepsilon}^+ + \boldsymbol{\varepsilon}^-, \quad \mathrm{tr}(\boldsymbol{\varepsilon}) = \mathrm{tr}^+(\boldsymbol{\varepsilon}) + \mathrm{tr}^-(\boldsymbol{\varepsilon}) \tag{15}$$

$$\boldsymbol{\varepsilon}^+ = \sum_{i\in A}\varepsilon_i\boldsymbol{n}_i\otimes\boldsymbol{n}_i, \quad A = \{i:\varepsilon_i \geq 0\}, \quad \mathrm{tr}^+(\boldsymbol{\varepsilon}) = \langle\mathrm{tr}(\boldsymbol{\varepsilon})\rangle \tag{16}$$

$$\boldsymbol{\varepsilon}^- = \sum_{i\in B}\varepsilon_i\boldsymbol{n}_i\otimes\boldsymbol{n}_i, \quad B = \{i:\varepsilon_i < 0\}, \quad \mathrm{tr}^-(\boldsymbol{\varepsilon}) = -\langle-\mathrm{tr}(\boldsymbol{\varepsilon})\rangle. \tag{17}$$

Accordingly the elastic part of the free energy is also divided into a positive part, which is corresponding to tension, where damage is fully active and a negative part

$$\psi_e(\boldsymbol{\varepsilon}, \boldsymbol{D}) = \underbrace{\frac{\lambda}{2}(1-g)[\mathrm{tr}^+(\boldsymbol{\varepsilon})]^2 + \mu(\boldsymbol{I}-\boldsymbol{D}):\boldsymbol{\varepsilon}_+^2}_{\psi_e^+} + \underbrace{\frac{\lambda}{2}(1-h_{\mathrm{tc}}\,g)[\mathrm{tr}^-(\boldsymbol{\varepsilon})]^2 + \mu(\boldsymbol{I}-h_{\mathrm{tc}}\,\boldsymbol{D}):\boldsymbol{\varepsilon}_-^2}_{\psi_e^-}. \tag{18}$$

The material parameter h_{tc} controls the degree of tension compression asymmetry (TCA) within the material: For the choice $h_{\mathrm{tc}} = 1$ the compression related part is damaged in an analogous manner to the tension related part (no crack-closure is considered). In contrast, the highest possible degree of TCA is achieved for $h_{\mathrm{tc}} = 0$. For this case, the compression related part is not damaged at all.

2.3 Gradient extension: micromorphic approach

The gradient extension is realized by adding one additional scalar micromorphic field variable according to Forest (2009). The additional global field variable α_χ is the counterpart to the local variable α and causes additional terms in the internal virtual work

$$g_{\text{int}} = \int_B \boldsymbol{\sigma} : \nabla^s \delta \boldsymbol{u} \, \mathrm{dV} + \int_B \left(\beta_\chi \, \delta \alpha_\chi + \boldsymbol{\xi} \cdot \nabla \delta \alpha_\chi \right) \mathrm{dV} \tag{19}$$

$$g_{\text{ext}} = \int_B \boldsymbol{f} \cdot \delta \boldsymbol{u} \, \mathrm{dV} + \int_{\partial B_t} \bar{\boldsymbol{t}} \cdot \delta \boldsymbol{u} \, \mathrm{dA} \tag{20}$$

with the Cauchy stress tensor $\boldsymbol{\sigma}$, the generalized stresses β_χ and $\boldsymbol{\xi}$, body force $\boldsymbol{f}$ an the prescribed traction vector $\bar{\boldsymbol{t}}$ on the boundary ∂B_t. $\delta \boldsymbol{u}$ and $\delta \alpha_\chi$ are suitable test functions. The micromorphic extension is neglected in the external virtual work, as Eq. (20) shows. Making use of the principle of virtual work

$$g_{\text{int}} \stackrel{!}{=} g_{\text{ext}} \tag{21}$$

the equations of linear momentum balance are obtained in the standard way

$$\text{div}(\boldsymbol{\sigma}) + \boldsymbol{f} = \boldsymbol{0} \quad \text{in} \quad B \tag{22}$$

$$\boldsymbol{\sigma}\,\boldsymbol{n} = \bar{\boldsymbol{t}} \quad \text{on} \quad \partial B_t \tag{23}$$

$$\boldsymbol{u} = \bar{\boldsymbol{u}} \quad \text{on} \quad \partial B_u. \tag{24}$$

For the additional field variable the micromorphic balance equation and the corresponding Neumann boundary condition on ∂B_Ξ are

$$\text{div}(\boldsymbol{\xi}) - \beta_\chi = 0 \quad \text{in} \quad B \tag{25}$$

$$\bar{\Xi} = \boldsymbol{\xi} \cdot \boldsymbol{n} = 0 \quad \text{on} \quad \partial B_\Xi. \tag{26}$$

In addition, the free energy of the local from Eq. (1) has to be extended by an additional micromorphic energy, which consists of two parts

$$\psi_{\text{micr}} = \frac{1}{2} H_\chi \left(\alpha_\chi - \alpha \right)^2 + \frac{1}{2} E l^2 \, \nabla \alpha_\chi \cdot \nabla \alpha_\chi. \tag{27}$$

The first part of Eq. (27) acts as a penalty energy which forces the micromorphic field variable α_χ to be as close as possible to the local variable α with the penalty parameter H_χ. The second part takes into account the energy stored by the gradiend of the micromorphic field variable α_χ.
With the additionally introduced micromorphic energy the expressions for the generalized stresses can then be derived

$$\beta_\chi = \frac{\partial \psi}{\partial \alpha_\chi} = H_\chi (\alpha_\chi - \alpha), \quad \boldsymbol{\xi} = \frac{\partial \psi}{\partial \nabla \alpha_\chi} = E l^2 \nabla \alpha_\chi. \tag{28}$$

3 Application and numerical results

Fassin et al. (2019a) showed that isotropic and anisotropic damage models yield to the same result if no diffusive damage occurs. Since this work focuses on the modeling of crack formation as shown in Fig. 1 and no diffusive damage.
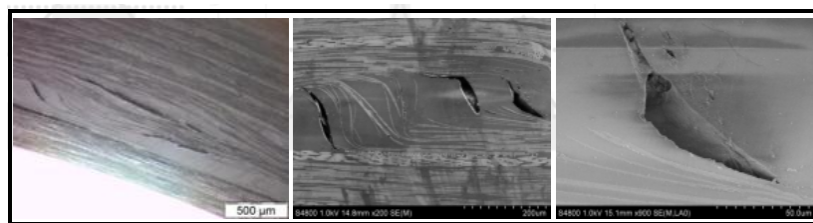

Fig. 1: Crack formations in the matrix material.

It is sufficient to make use of the simplified gradient-extended isotropic damage model for the simulations of the epoxy matrix on the microlevel.

3.1 1-D isotropic damage

In order to identify relevant material parameters from the more classical fracture mechanic theory like the strain energy release rate or stress at fracture, the first variation of the free energy functional with respect to D (Eq. (29)-(31)) provides the essential criteria. The procedure is similar to Francfort and Marigo (1998), Bourdin et al. (2008) and Pham et al. (2011).
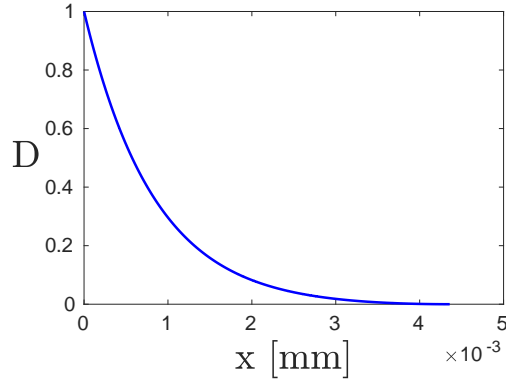
Fig. 2: Solution for D.

With the evaluation of Eq. (29) the strain energy release rate G_c can be formulated dependent on the internal length l, which controls the thickness of the damage localization zone.

$$\delta_D \int_V \psi dV = 0 \rightarrow \quad \ldots \quad \frac{dE}{dA} = \sqrt{2E} \, 2l \int_0^1 \sqrt{w(D)} dD = G_c \tag{29}$$

$$\psi = w(D) + \frac{1}{2} E l^2 \nabla D \cdot \nabla D \tag{30}$$

$$w(D) = Y_0^c D + \frac{1}{2} K_1 D^2 \tag{31}$$

The damage criterion provides a useful criterion for the stress at fracture σ_c which is corresponding to the damage threshold Y_0^c.

$$\Phi = 0 \rightarrow \quad \psi_0(\varepsilon) = Y_0^c \quad \rightarrow \sqrt{2E\, Y_0^c} = \sigma_c \tag{32}$$

$$Y_0^c + K_1 D - E l^2 D'' = 0 \quad \text{with} \quad D(x_0) = D'(x_0) = 0. \tag{33}$$

The solution of Eq. (33) is plotted in Fig. 2. $2x_0$ represents the whole crack width or rather the thickness of the damage localization zone. Thus, the strain energy release rate G_c, stress at fracture σ_c and the crack width x_0 can be controlled at the same time.

3.2　Unit cell simulations with variations of the fracture toughness

As numerical example a quadratic unit cell with 60% fiber and 2% pore volume fraction is considered (see Fig. 3). Periodic boundary conditions are defined. It is noted that the unit cell can't be considered as statistically representative. The material parameters are set such that no damage will occurs in the fiber material with E=220000 N/mm^2, ν=0.2, Y_0^c=∞ Nmm/mm. For the matrix material the parameters E=3000 N/mm^2, ν=0.3, K_1=100.0 Nmm/mm^3, H_χ=10^6 Nmm/mm^3, l=1.5552 · 10^{-4} mm, Y_0^c=1.1258 Nmm/mm^3 are used.
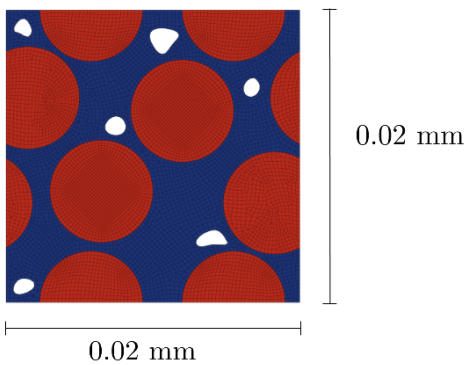

0.02 mm

0.02 mm

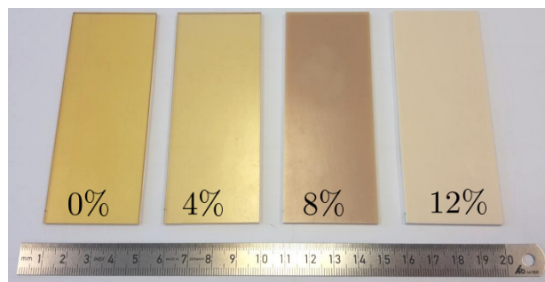Fig. 3: Unit cell geometry.

0%　　4%　　8%　　12%

Fig. 4: Specimen with variation of CSR particles.

In this first example the variation of the fracture toughness is shown. In reality, soft and elastic Core-Shell-Rubber particles (CSR) are embedded in the epoxy matrix. With increasing volume fraction of CSR particles (Fig. 4) the fracture toughness increases and the limit stress σ_c decreases. The new material parameters in Tab. 1 for varying CSR volume fraction are identified with the criteria of subsection 3.1.

The limit stress σ_c is decreasing for increasing CSR fraction. With Eq. (32) the initial damage threshold (the last column of Tab. 1) has to decrease, in analogy. The crack width x_0 for the given geometry in Fig. 3 remains constant.

The average stress over the average strain is plotted for the load case $\varepsilon_{yy} > 0$ for each CSR variation in Fig. 5 and shows the increasing maximum stress for increasing matrix fracture toughness.

Tab. 1: List of material parameters for matrix material with varying CSR volume fraction.

CSR	E [N/mm^2]	K_1 [Nmm/mm^3]	l [mm]	Y_0^c [Nmm/mm^3]
0%	3000	100.0	1.5552e-04	1.1258
4%	2752	200.0	1.9877e-04	0.9419
8%	2604	300.0	2.1169e-04	0.8619
12%	2440	350.0	2.2885e-04	0.8133
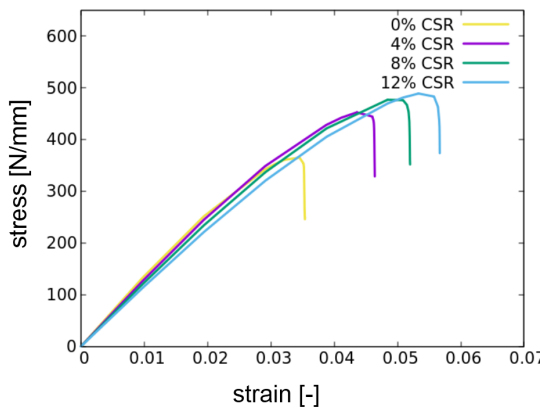
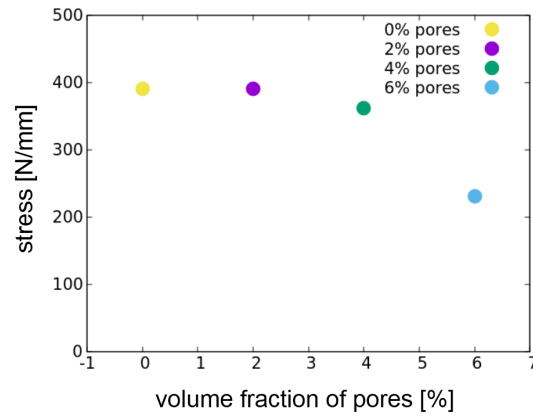Fig. 5: Average stress over average strain for varying CSR volume fraction.

Fig. 6: Maximum average stress over pore volume fraction.

In this case, the conventional scale transition criteria aren't satisfied, i.e., the depicted behavior is related to the unit cell (not the composite) and thus only qualitative. While the Young's modulus for the matrix material is decreasing (second column in Tab. 1) and the fracture toughness which is corresponding to the energy release rate G_c is increasing, it is reasonable that the maximum average stress of the unit cell increases, too.

3.3 Unit cell simulations with variations of pore volume

In the next numerical example the volume fraction of pores is modified with 0%, 2%, 4% and 6%. The initial material parameter set is taken from subsection 3.2 for the matrix material without incorporation of CSR particles (0% CSR volume fraction). Geometry, fiber volume fraction as well as fiber material parameters stay the same.

Representing only first qualitative observations these UC simulations show that with increasing volume fraction of pores the average maximum stress is decreasing, which is visualized in Fig. 6. Crack initiation starts in the matrix material near a pore and propagates along the interface, but does not pass through the rubber particles.

Furthermore Fig. 6 emphasizes that 2% volume fraction of pores does not have a remarkable influence on the maximum average stress. This is different between 4% and 6% volume fraction where a bigger difference of the average stress is noticeable. This observation has to be investigated with using more representative unit cells.

4 Conclusion

In the present work, an anisotropic gradient-extended brittle damage framework of Fassin et al. (2019a) was presented. In addition, the model enables tension compression asymmetry (crack-closure) extension recently published in Fassin et al. (2019b). The numerical examples make use of the simplification of the model to isotropic damage.

The two numerical examples of unit cell simulations, where first the fracture toughness and second the pore volume fraction was varied, were shown. Both results demonstrate reasonable overall response. Though for statistical representation more unit cell simulations have to be done considering bigger unit cells. For the purpose of investigation of the performance of carbon reinforced epoxy resin the next (macro) scale has to consider anisotropic damage with crack-closure consideration for a more realistic material response.

Acknowledgment and Funding Information

References

B. Bourdin, G. A. Francfort, and J.-J. Marigo. The variational approach to fracture. *Journal of elasticity*, 91(1-3):5–148, 2008.

M. Fassin, R. Eggersmann, S. Wulfinghoff, and S. Reese. Efficient algorithmic incorporation of tension compression asymmetry into an anisotropic damage model. *Computer Methods in Applied Mechanics and Engineering*, 2019b.

M. Fassin, R. Eggersmann, S. Wulfinghoff, and S. Reese. Gradient-extended anisotropic brittle damage modeling using a second order damage tensor–theory, implementation and numerical examples. *International Journal of Solids and Structures*, 167: 93–126, 2019a.

S. Forest. Micromorphic approach for gradient elasticity, viscoplasticity, and damage. *Journal of Engineering Mechanics*, 135 (3):117–131, 2009.

G. A. Francfort and J.-J. Marigo. Revisiting brittle fracture as an energy minimization problem. *Journal of the Mechanics and Physics of Solids*, 46(8):1319–1342, 1998.

P. Ladeveze and J. Lemaitre. Damage effective stress in quasi unilateral conditions. In *16th International congress of theoretical and applied mechanics, Lyngby, Denmark*, 1984.

K. Pham, H. Amor, J.-J. Marigo, and C. Maurini. Gradient damage models and their use to approximate brittle fracture. *International Journal of Damage Mechanics*, 20(4):618–652, 2011.